Multivoltage-Vector-Modulation-Based Integrated Direct Torque Control of Dual in-Wheel PM Motors for Distributed Drive Electric Vehicles

Zhaoheng Wang, Xiaoyong Zhu, *Member, IEEE*, Lei Xu, *Member, IEEE*, Wen-Hua Chen, *Fellow, IEEE*, Qiyuan Liu, and Li Quan

***Abstract*—To improve the coordinate control performance of the multiple motors in the distributed drive (DD) electric vehicle (EV) system, an integrated direct torque control with multiple voltage vector (MVV) modulation is developed and implemented in this article. It focuses on the integrated modulation principle considering dynamic operating demands and interaction between the independent drive wheels, where the frequency ratio integrated modulation and virtual vector integrated modulation are proposed and investigated. And then, a 1/2 DD system with the dual in-wheel permanent magnet (DIW-PM) motors which is represented in the front and rear drive wheels is selected as the control example. Based on the six-leg inverter, the dual in-wheel permanent magnet motor drive system is established and the mathematic model is derived. The different modulation methods are discussed and compared. Finally, the experiments are conducted on the DD system with two different power levels and configurations in-wheel PM motors, and the experimental results are presented to verify the effectiveness of the proposed integrated direct torque control method for the EV distributed drive systems.**

***Index Terms*—Distributed drive (DD), in-wheel permanent magnet (PM) motor, integrated direct torque control, multivoltage-vector modulation.**

I. Introduction

DISTRIBUTED drive (DD) system that features short transmission chain, compact structure, improved tire adhesion distribution and high drive efficiency, which can significantly improve the vehicle dynamics performance and energy utilization of electric vehicles (EV), has received widespread attentions [1], [2]. The DD system normally comprises two or more motors with different output power to realize the direct drive of the wheels, where the need for an intermediate differential to transmit torque is eliminated [3]. To control the multiple motor systems, a hierarchical master-slave controller through communication protocols is generally adopted [4], as shown in Fig. 1. Yet, with the rapid iteration of intelligent driving technology, high computing performance of the upper-level decision controllers and the layered controllers is required to implement advanced intelligent algorithms [5]. The multiprocessor redundancy design and motor controller layer with more autonomous decision-making capability which can reduce the workload of the upper-level controller and improve the reliability of the system have become the mainstream architectures of the EV systems [6], [7].

For the motor control layer with autonomous decision-making, the collaborative control of the multiple motors is one of the key challenges in the DD control system. It should be both independently respond to the driving demands of each wheel and achieve synchronization of the multiple wheels without influencing on the single wheel. Specifically, on the one hand, the changes in driving conditions, operating modes, and structural parameters have a huge impact on the coordination control. When there are coupling or overlapping motor drive systems in the vehicle chassis that lack coordination control, it would inevitably lead to deterioration of vehicle comprehensive performance under the complex driving conditions [8]. In face of the complex and ever-changing operating conditions, it is easy to experience disturbances in the internal parameters of the drive motors and external load disturbances, leading to a decrease in the control performance of multiple drive motors, resulting in speed errors, uncoordinated speed response, and mutual dragging or sliding of the drive wheels.

On the other hand, the control strategy of a single in-wheel motor also directly affects the response speed and dynamic performance of the DD system. Due to varying road conditions, the motor control strategy may struggle to promptly account for the combined outputs of all wheels when responding to these disturbances [9]. This may result in temporary speed discrepancies,

Received 8 July 2024; revised 13 September 2024; accepted 2 October 2024. This work was supported in part by the Key International (Regional) Cooperative Research Programs of National Natural Science Foundation of China under Grant 52320105009, and in part by the National Natural Science Foundation of China under Grant 51937006. *(Corresponding author: Xiaoyong Zhu.)*

Zhaoheng Wang, Xiaoyong Zhu, Lei Xu, Qiyuan Liu, and Li Quan are with the School of Electrical and Information Engineering, Jiangsu University, Zhenjiang 212013, China (e-mail: 2222207035@stmail.ujs.edu.cn; zxyff@ujs.edu.cn; leixu@ujs.edu.cn; 2212307019@stmail.ujs.edu.cn; quanli@ujs.edu.cn).

Wen-Hua Chen is with the Department of Aeronautical and Automotive Engineering, Loughborough University, LE11 3TU Loughborough, U.K. (e-mail: w.chen@lboro.ac.uk).

Digital Object Identifier 10.1109/TIE.2024.3482000

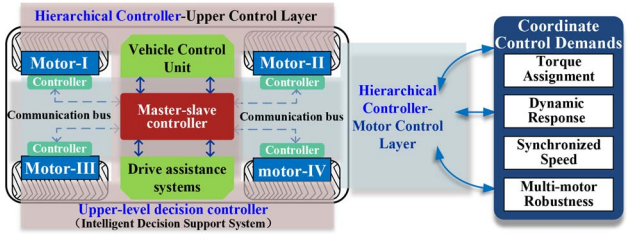

Fig. 1. The control architecture in the distributed drive systems.

uneven distribution of torque, and other instabilities within the system, ultimately reducing the riding comfort. Therefore, how to achieve speed synchronization and dynamic torque assignment and response of in-wheel motors, how to improve the intelligent control performance of the motor control layer, and how to satisfy the complex driving conditions and autonomous decision-making requirements have become hotspots and key issues in the research field of distributed in-wheel motor drive electric vehicles.

To solve the above issues, various control theories and methods have been applied for the multiple motor control system. The torque assignment control strategies with the wheel operating status evaluation [10], [11], neural network controller [12], and state error observer [13] are proposed for the DD system. Furthermore, a torque distributor with motor drive control and regenerative braking control is proposed in [14]. Furthermore, based on the MPC of the tire models, the torque distributor is established in [15], [16], [17] where the cost function of each wheel is constructed on the target of slip rate. The above control strategies have laid the foundation for the DD system. Indeed, the existing control techniques for the DD system generally treat the traction motors as moving points, neglecting the characteristics of a single motor and failing to consider them as an overall coordinated target with motion characteristics. It results in low efficiency and being susceptible to operating condition of the motor controller, and consequently the DD system cannot respond to changes in the environment or operating conditions efficiently [18]. Meanwhile, it also increases computational burden on the upper layer controllers.

In terms of the single motor control, in general different control methods such as field-oriented control (FOC), direct torque control (DTC), and model predictive current control (MPCC). Yield different control characteristics [19], [20], and consequently may result in different operating characteristics of the motor. Moreover, without considering the collaborative control strategy, the single motor control only has unidirectional characteristics, and does not respond to the variation of the other in-wheel motors. It also makes the correctness and real-time performance of the upper layer controller decisions in traditional collaborative control systems particularly important. Hence, how to coordinate control the individual in-wheel traction motors with different control methods and possibly consider different motor power levels with optimal combined power characteristic output is a key issue that needs to be urgently addressed in the DD system.

In response to the demand of the collaborative control in the electric vehicle distributed drive system, based on the direct torque control, the integrated modulation concept of the multiple in-wheel motors is proposed in this article. By changing the traditional centralized controller and respective in-wheel motor controllers to an integrated direct torque controller with multivoltage-vector (MVV) modulation, the front and rear in-wheel motors are drive together, where the information interaction chain is shortened and the coordinated control efficiency and overall controller robustness will be improved. Simultaneously, by adopting a six-leg inverter coupled with the integrated modulation concept, the overall vehicle smoothness and handling stability are improved. Moreover, it also focuses on the effects of the integrated direct torque control on the dynamic performance of the DD system, including the synchronous performance and anti-interference performance of the dual in-wheel motors, and analyzes the utilization rate of bus voltage and harmonic suppression effect.

This article is organized as follows. The integrated modulation control concept is proposed for the DD system. A 1/2 distributed drive electric vehicle system is selected as an example, which consists of dual in-wheel permanent magnet (DIW-PM) motors. In addition, the mathematical model of the DIW-PM motors is established in Section II. In Section III, the integrated direct torque control strategy with the multiple voltage vector modulation is proposed and investigated. The MVV modulation strategy based on the frequency ration and virtual vector are presented and derived in detail. In sequence, based on the experimental setups, the different modulation strategies are discussed and compared in Section IV. Finally, the conclusions will be drawn in Section V.

II. Integrated Modulation Control Concept and Mathematical Model of the DIW-PM Motors

A. Integrated Modulation Control Concept

With the increasingly complex traffic conditions and performance demanding, higher drive requirements have been put forward for the EV's drive motors. For the China light vehicle test cycle (CLTC) [21], [22], the light-duty vehicles face multiple frequent and continuous acceleration, deceleration, and start stop states, which are more evident in commercial vehicles, with acceleration and deceleration frequencies accounting for 28%. In addition, frequent speed adjustments in the mid and high-speed operating conditions account for 30%. These demanding operations pose higher drive requirements for the coordinated control of multiple in-wheel motors in the DD system.

Moreover, in the DD system with four in-wheel motors traction, the road conditions of the front and rear in-wheel motors may be inconsistent under straight driving conditions. When the performance of the front and rear in-wheel motors are inconsistent, such as moment of inertia and power level, the poor dynamic synchronization performances are obtained at the starting, changing speed and being disturbed operating conditions, which can lead to side slip, chatter, serious tire wear, and other adverse consequences. To avoid the mutual dragging, higher dynamic response and coordination control capacity of the in-wheel motor drive systems with independent controllers are strictly required.

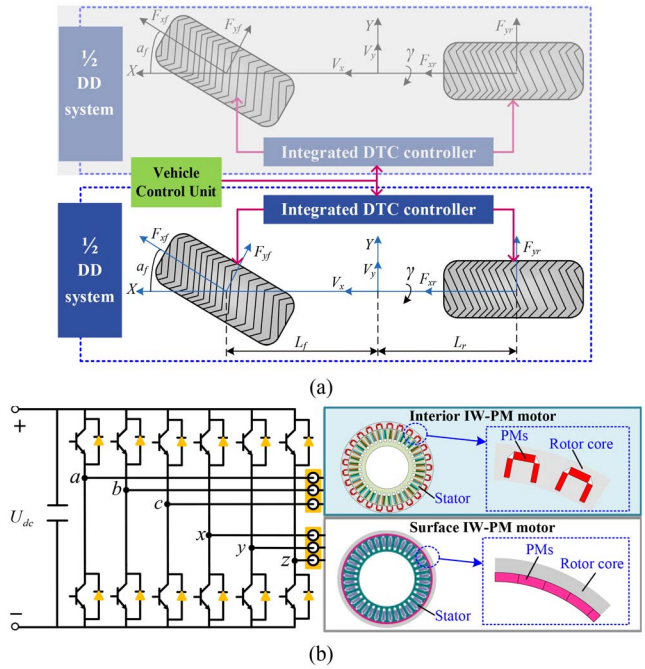

Fig. 2. Two degree of freedom lateral dynamics model. (a) Two degree of freedom lateral dynamics model. (b) Six-leg inverter-motor system topology.

Since the fast response and coordinated control are the core demands of the DD systems, it is significant to propose a control method that not only satisfies the high dynamic performance of a single motor drive, but also achieves rapid cooperation among multiple in-wheel motors. Furthermore, it is crucial that the control requirements and performance objectives are no longer just for a single in-wheel motor, but for the multiple in-wheel motors which are controlled as a whole under the complex operating conditions.

Hence, in this article, the integrated modulation control concept is proposed where two or more motors are controlled by one controller with different power converters. The drive signals of these motor power converters are modulated uniformly and directly, rather than through the traditional method of separate and independent control. As shown in Fig. 2(a), a 1/2 DD system with dual in-wheel motors is considered as the case study to illustrate our control design method where the dual in-wheel motors are integrated and controlled. In the 1/2 DD system, an in-wheel interior PM motor and an in-wheel surface PM motor with different power levels are taken, which are utilized as the front and rear in-wheel drive respectively. The six half-bridges, comprising two three-leg inverters, are employed to drive the two motors. Furthermore, a controller is employed for the centralized integrated control of the dual in-wheel motors.

B. Mathematical Model of the DIW-PM Motors

According to the traditional two motor drive system [23], the DIW-PM motors are independent of each other in space and the mathematical model of the DIW-PM motors in the α/β coordinate systems are parallel. To simplify the construction of the mathematical model, the three-phase windings of the two

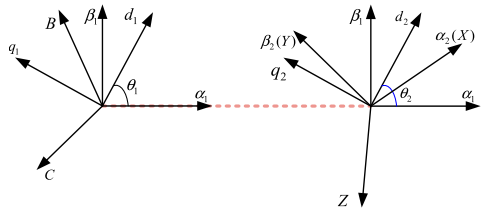

Fig. 3. Frame transformation of the DIW-PM motors.

motors are virtually shifted by 30°. Hence, the double motor Clarke–Park six-dimensional transformation matrix is constructed

$$T_{3s/2s} = \begin{bmatrix} T_1 & 0 \\ 0 & T_2 \end{bmatrix} \tag{1}$$

$$T_1 = \frac{2}{3}\begin{bmatrix} \cos\theta & \cos(\theta-2\pi/3) & \cos(\theta+2\pi/3) \\ -\sin\theta & -\sin(\theta-2\pi/3) & -\sin(\theta+2\pi/3) \\ 1/2 & 1/2 & 1/2 \end{bmatrix} \tag{2}$$

$$T_2 = \frac{2}{3}\begin{bmatrix} \cos(\theta-\pi/6) & \cos(\theta-5\pi/6) & \cos(\theta+\pi/2) \\ -\sin(\theta-\pi/6) & -\sin(\theta-5\pi/6) & -\sin(\theta+\pi/2) \\ 1/2 & 1/2 & 1/2 \end{bmatrix}. \tag{3}$$

As shown in Fig. 3, T_2 lags behind T_1 with an electrical angle of 30°. Under the α_1-β_1 coordinate system, T_1 is the static coordinate transformation of the motor-I. And, T_2 corresponds to the motor-II under the α_2-β_2 coordinate system.

The equations for the current of dq-axis, the dq-axis flux vectors, and electromagnetic torque of the DIW-PM motors are as follows:

$$\begin{bmatrix} i_{d1} & i_{q1} & i_{d2} & i_{q2} \end{bmatrix}^T = T_{3s/2s}\begin{bmatrix} i_{a1} & i_{b1} & i_{c1} & i_{a2} & i_{b2} & i_{c2} \end{bmatrix}^T \tag{4}$$

$$\begin{bmatrix} \psi_{d1} \\ \psi_{q1} \\ \psi_{d2} \\ \psi_{q2} \end{bmatrix} = \begin{bmatrix} L_{\mathrm{d1}} & 0 & 0 & 0 \\ 0 & L_{\mathrm{q1}} & 0 & 0 \\ 0 & 0 & L_{\mathrm{d2}} & 0 \\ 0 & 0 & 0 & L_{\mathrm{q2}} \end{bmatrix}\begin{bmatrix} i_{d1} \\ i_{q1} \\ i_{d2} \\ i_{q2} \end{bmatrix} + \begin{bmatrix} 1 \\ 0 \\ 1 \\ 0 \end{bmatrix}\psi_f \tag{5}$$

$$T_{e1,2} = 1.5\left(\begin{bmatrix} \psi_{f1}i_{q1} & 0 \\ 0 & \psi_{f2}i_{q2} \end{bmatrix} + \begin{bmatrix} L_{d1}-L_{q1} & 0 \\ 0 & L_{d2}-L_{q2} \end{bmatrix}\begin{bmatrix} i_{d1}i_{q1} & 0 \\ 0 & i_{d2}i_{q2} \end{bmatrix}\right)\begin{bmatrix} p_1 \\ p_2 \end{bmatrix}. \tag{6}$$

III. Principle of the Integrated Modulation-Based Direct Torque Control

According to the integrated modulation control concept, an integrated direct torque control with MVV modulation is proposed for the DIW-PM motors, as shown in Fig. 4.

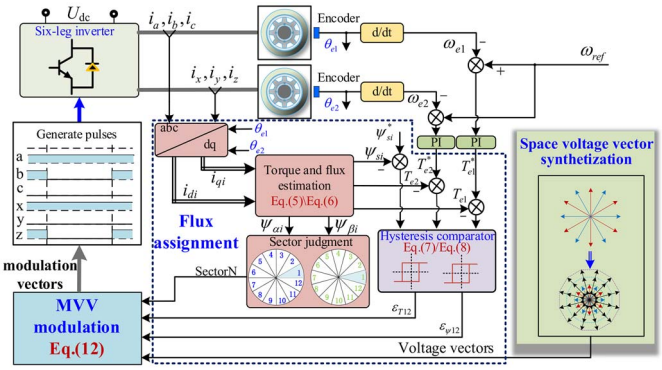

Fig. 4. Block diagram of the integrated direct torque control for DD system.

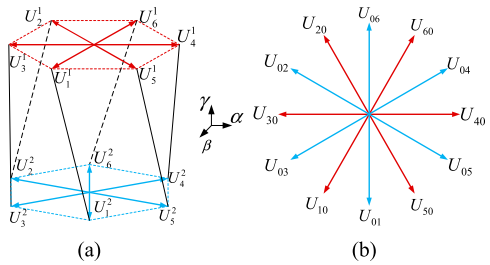

Fig. 5. The original space voltage vectors of DIW-PM motors. (a) 3-D space voltage vectors. (b) 2-D voltage vectors.

The integrated direct torque control mainly includes space voltage vector synthetization, flux assignment, and MVV modulation. It should be noted that the driving control of a single in-wheel motor is no longer an independent DTC control, but a centralized and integrated DTC control. It is important to highlight that MVV modulation, which serves as a core component, is preconfigured in practical applications and does not impose an additional computational burden during real-time vehicle operations. Furthermore, the integrated modulation control concept enables DIW-PM motors to utilize a shared MVV modulation database, thereby minimizing the number of lookup steps required in the control process and further improving the fault tolerance and robustness of distributed drive systems.

A. Space Voltage Vector Synthetization

In the 1/2 DD system, the integrated modulation control concept constrains the DIW-PM motors motion, forming a three-dimensional subspace shown in Fig. 5, which serves as the magnetic coupling boundary. And the two-dimensional subspace is shown in Fig. 5(b).

According to the integrated modulation concept, the magnetic coupling constraint makes the dual motors considered as a unified single motor. Therefore, combining Fig. 3 and the vector space decoupling transformation matrix of multiphase motors [24], [25], the original voltage vector modulation in Fig. 5(b) forms the α_1-β_1 subspace and fifth harmonic α_5-β_5 subspace shown in Fig. 6. It is worth noting that six half-bridges, comprising two three-leg inverters, has the capability to generate 64 distinct switching states. Hence, the voltage vectors with amplitude

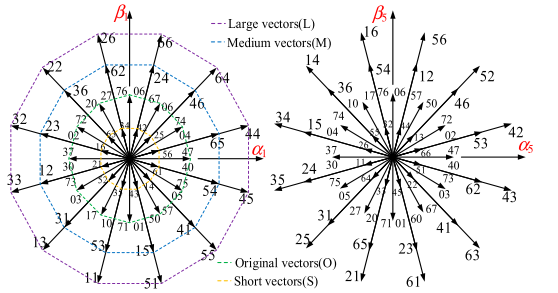

Fig. 6. Voltage vectors synthetization in α_1-β_1 and α_5-β_5 subspaces.

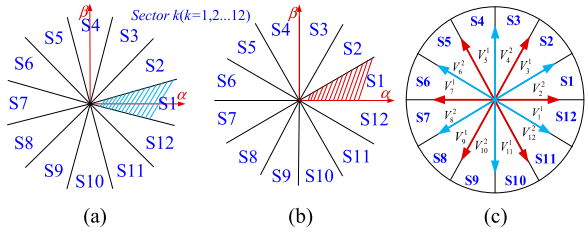

Fig. 7. Flux sector assignment method and original voltage vectors. (a) Method-I. (b) Method-II. (c) Original voltage vectors.

$1/3U_{dc}$ represent the 12 original voltage vectors in Fig. 5(b) corresponding to 24 switch states of the six-leg inverter, where exist a set of three-phase winding switch states that are either 0 or 7, representing voltage vectors with an amplitude of 0. Those original voltage vectors are synthesized in pairs to form remaining 36 voltage vectors in Fig. 6 (e.g., V_{64} is composed of U_{04} and U_{60}) which also includes 4 zero vectors located at the origin position. The vectors in the α_1-β_1 coordinate correspond to the vectors in the fifth harmonic α_5-β_5 coordinate, and each voltage vector is numbered in decimal as $S_aS_bS_cS_xS_yS_z = 110\ 110 = V_{66}$. Moreover, voltage vectors can be categorized into four distinct types based on each magnitude: large vectors with an amplitude of $0.644U_{dc}$; medium vectors with an amplitude of $0.471U_{dc}$; original vectors with an amplitude of $U_{dc}/3$ and short vectors with an amplitude of $0.173U_{dc}$.

B. Flux Assignment

In addition, to manipulate the synthesized voltage vectors, it is imperative to select an appropriate flux sector assignment method, which directly affects the selection of the voltage vector. Therefore, to clarify the impact of individual voltage vector, the voltage vector plane is segmented into 12 sectors as shown in Fig. 7, which includes two methods of flux sector assignment. It should be noted that inappropriate sector assignment can lead to ambiguity in the selection of voltage vectors, resulting in ineffective tracking of torque and flux loops. Therefore, in the case of the voltage vector expressed in Fig. 5(b), the method-II is employed for sector assignment, which is shown in Fig. 7(c). Similarly, for the virtual vector of MVV modulation illustrated in Fig. 9, method-I is selected. Furthermore, to simplify the naming of the voltage vectors, the voltage vector in Fig. 7(c) is equivalent to that in Fig. 6 (e.g., $V_1{}^1$ represents U_{40}).

Combining the principle of optimal flux sector assignment, the sector in which the flux is located at any time can be obtained by

TABLE I
SWITCH TABLE OF THE MVV MODULATION STRATEGY

Sector k (k = 1, 3, 5, 7, 9, 11)	$\varepsilon_{T12}=11$	$\varepsilon_{T12}=10$	$\varepsilon_{T12}=01$	$\varepsilon_{T12}=00$
$\varepsilon\psi_{12}=11$	$V_{k+2}^1V_{k+3}^2$	$V_{k+2}^1V_{k-1}^2$	$V_{k-2}^1V_{k+3}^2$	$V_{k-2}^1V_{k-1}^2$
$\varepsilon\psi_{12}=10$	$V_{k+2}^1V_{k+5}^2$	$V_{k+2}^1V_{k-3}^2$	$V_{k-2}^1V_{k+5}^2$	$V_{k-2}^1V_{k-3}^2$
$\varepsilon\psi_{12}=01$	$V_{k+4}^1V_{k+3}^2$	$V_{k+4}^1V_{k-1}^2$	$V_{k-4}^1V_{k+3}^2$	$V_{k-4}^1V_{k-1}^2$
$\varepsilon\psi_{12}=00$	$V_{k+4}^1V_{k+5}^2$	$V_{k+4}^1V_{k-3}^2$	$V_{k-4}^1V_{k+5}^2$	$V_{k-4}^1V_{k-3}^2$
Sector k (k = 2, 4, 6, 8, 10, 12)	$\varepsilon_{T12}=11$	$\varepsilon_{T12}=10$	$\varepsilon_{T12}=01$	$\varepsilon_{T12}=00$
$\varepsilon\psi_{12}=11$	$V_{k+3}^1V_{k+2}^2$	$V_{k+3}^1V_k^2$	$V_{k-1}^1V_{k+2}^2$	$V_{k-1}^1V_k^2$
$\varepsilon\psi_{12}=10$	$V_{k+3}^1V_{k+4}^2$	$V_{k+3}^1V_{k-4}^2$	$V_{k-1}^1V_{k+4}^2$	$V_{k-1}^1V_{k-4}^2$
$\varepsilon\psi_{12}=01$	$V_{k+5}^1V_{k+2}^2$	$V_{k+5}^1V_k^2$	$V_{k-3}^1V_{k+2}^2$	$V_{k-3}^1V_k^2$
$\varepsilon\psi_{12}=00$	$V_{k+5}^1V_{k+4}^2$	$V_{k+5}^1V_{k-4}^2$	$V_{k-3}^1V_{k+4}^2$	$V_{k-3}^1V_{k-4}^2$

estimating the flux. And the flux estimation can be determined by performing a coordinate transformation using (5).

In addition, to effectively regulate the torque and flux control loop, it is imperative to acquire the tolerance values of torque and flux by hysteresis comparators. The torque and flux amplitudes are adjusted through hysteresis comparators, where the differences between the expected value and the feedback value are compared with the upper and lower limits of the hysteresis comparator to determine the signals for increasing or decreasing torque and flux, and the hysteresis comparators are expressed as

$$\varepsilon_{T12}=\begin{cases}11,(T_{e1}^*-T_{e1}>0.001)\&(T_{e2}^*-T_{e2}>0.001)\\10,(T_{e1}^*-T_{e1}>0.001)\&(T_{e2}^*-T_{e2}<-0.001)\\01,(T_{e1}^*-T_{e1}<-0.001)\&(T_{e2}^*-T_{e2}>0.001)\\00,(T_{e1}^*-T_{e1}<-0.001)\&(T_{e2}^*-T_{e2}<-0.001)\end{cases} \tag{7}$$

$$\varepsilon_{\psi 12}=\begin{cases}11,\left(|\psi_{s1}^*|-|\psi_{s1}|>0.0001\right)\&\left(|\psi_{s2}^*|-|\psi_{s2}|>0.0001\right)\\10,\left(|\psi_{s1}^*|-|\psi_{s1}|>0.0001\right)\&\left(|\psi_{s2}^*|-|\psi_{s2}|<-0.0001\right)\\01,\left(|\psi_{s1}^*|-|\psi_{s1}|<-0.0001\right)\&\left(|\psi_{s2}^*|-|\psi_{s2}|>0.0001\right)\\00,\left(|\psi_{s1}^*|-|\psi_{s1}|<-0.0001\right)\&\left(|\psi_{s2}^*|-|\psi_{s2}|<-0.0001\right)\end{cases},$$

$$|\psi_{si}|=\sqrt{\psi_{\alpha i}^2+\psi_{\beta i}^2} \tag{8}$$

where T_{ei} (i = 1, 2) are calculated by (6). And generally, $|\psi_{si}^*|$ (i = 1, 2) are equal to the amplitude of the permanent magnet's flux.

C. MVV Modulation Strategy

According to voltage vector synthetization in Fig. 6, and the flux assignment which includes current flux sector, the torque and flux output signals derived through hysteresis comparators, the multiple voltage vectors are selected in the Table I (e.g., $V_1{}^1V_2{}^2$ represents V_{44}), where the control signals for electromagnetic torque and stator flux are denoted as ε_{Ti} and $\varepsilon_{\psi i}$, respectively.

It should be noted that the output of the hysteresis comparator can be arbitrarily combined to meet the differential or synchronization requirements of the DIW-PM motors. Subsequently, the optimal voltage vector is selected by MVV modulation strategy according to Table I, effectively distributing the driving power for the dual motors. Therefore, this flexible MVV modulation strategy is sufficient to cope with complex and variable vehicle operating circumstances.

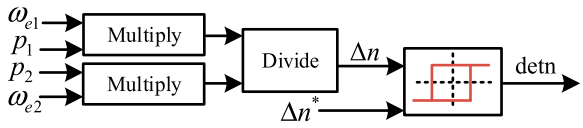

Fig. 8. Frequency ratio judgment.

1) MVV Modulation Based on Frequency Ratio: In general, in-wheel motors with different parameters are employed to improve the adaptability of vehicles to complex road conditions in a DD system. Nevertheless, the synchronization performance of the wheels during variable speed process is poor, necessitating precise coordination of the controller, particularly in straight driving scenarios. Therefore, to further improve the synchronization performance of the process, based on the switch table of the multiple voltage vectors, the frequency ratio of MVV (FR-MVV) modulation is investigated, as shown in Fig. 8. Additionally, a hysteresis comparator is introduced in (9), with the threshold B_f determined by the sampling precision of the vehicle's electronic control unit and the computational complexity of the control system. The threshold B_f is equal to 0.001

$$\text{detn}=\begin{cases}1 & \Delta n^*-\Delta n\geq B_f\\0 & \Delta n^*-\Delta n<-B_f.\end{cases} \tag{9}$$

By taking the speed of motor-II as a reference, when the motor-I lags behind, indicated by detn = 1, the $k+1$ vector should be used for acceleration instead of the vector specified in the Table I. However, this approach leads to a significant decrease in the amplitude of flux, which fails to meet the performance criteria. On the other hand, when the motor-I speed exceeds, represented by detn = 0, the $k-1$ vector should be employed for deceleration when $\varepsilon_{Ti}=1$, ensuring compliance with flux and torque requirements while achieving the desired deceleration for motor-I. Based on the aforementioned analysis, the switch table of FR-MVV is established as shown in Table II.

2) MVV Modulation Based on Virtual Vector: Although the application of the switch tables for the MVV modulation strategy and FR-MVV can effectively control the DIW-PM motors to face various working conditions, FR-MVV is only suitable for straight driving condition. On the other hand, the voltage vectors selected in the Tables I and II include the long vectors, medium vectors, and short vectors. This has the dual effects of reducing the utilization rate of bus voltage, which is easily influenced by the selected voltage vector magnitude, and potentially increasing losses due to the lack of harmonic flux control in the α_5–β_5 subspace. These factors lead to an increase in the harmonic content of the stator current, impacting overall system efficiency. Hence, to enhance the efficiency of bus voltage utilization, mitigate current harmonics, and simultaneously accommodate diverse intricate driving scenarios, the virtual vector of MVV (VV-MVV) modulation is proposed.

TABLE II
SWITCH TABLE OF THE FR-MVV

Sector k (k = 1, 3, 5, 7, 9, 11)	detn = 1	detn = 0
$\varepsilon\psi_1 = 0$, $\varepsilon_{T1} = 1$	Unchanged	V_{k+4}^1
$\varepsilon\psi_2 = 1$ $\varepsilon_{T2} = 1$	Unchanged	V_{k+2}^1
Sector k (k = 2, 4, 6, 8, 10, 12)	detn = 1	detn = 0
$\varepsilon\psi_1 = 0$, $\varepsilon_{T1} = 1$	Unchanged	V_{k+3}^1
$\varepsilon\psi_2 = 1$ $\varepsilon_{T2} = 1$	Unchanged	V_{k+1}^1

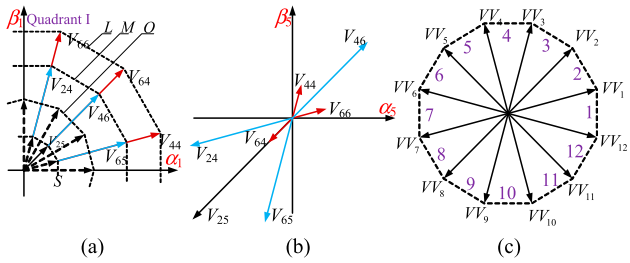

Fig. 9. Twelve virtual voltage vectors synthesized in α_1-β_1 subspaces. (a) α_1-β_1 Subspace. (b) α_5-β_5 Subspace. (c) Virtual vectors.

Due to the nonzero sequence component of voltage vectors in the fifth harmonic α_5-β_5 subspace, the voltage vector selected in the α_1-β_1 subspace exerts a malignant impact on the α_5-β_5 subspace. To enhance the magnitude of the virtual vector while reducing the harmonic content, two vectors are selected from Fig. 6 to synthesize a virtual vector, so that the magnitude of the virtual vector synthesized in the fifth harmonic α_5-β_5 subspace is zero. Consequently, the voltage vectors used to synthesize the virtual vectors should be aligned in the same direction in the α_1-β_1 subspace, while they should be opposite in the α_5-β_5 subspace. Taking the voltage vectors in quadrant I of the α_1-β_1 subspace as an example, as shown in Fig. 9(a), the large vector (e.g., V_{44}, V_{64}, and V_{66}) and the medium vectors (e.g., V_{65}, V_{46}, and V_{24}) are collinear and able to eliminate the harmonic components when synthesizing the virtual vectors. Although it is possible to use the short vector V_{25} and medium vector V_{46} for synthesizing a virtual vector, the smaller magnitude of the synthesized virtual vector leads to a decrease in the bus voltage utilization. Therefore, the optimal virtual vectors are composed of the long and medium vectors.

To synthesize the virtual vectors, the principle of voltage-second balance can be explained as follows:

$$\begin{cases} |VV_{S1}|T_S = |V_L|K_L T_S + |V_M|K_M T_S \\ \qquad\quad = 0.644U_{\rm dc}K_L T_S + 0.471U_{\rm dc}K_M T_S \\ |VV_{S5}|T_S = |V_M|K_L T_S - |V_L|K_M T_S \\ \qquad\quad = 0.471U_{\rm dc}K_L T_S - 0.644U_{\rm dc}K_M T_S. \end{cases} \tag{10}$$

where K_L and K_M represent the duty cycle of the long and medium vectors in the control cycle T_s respectively, and $K_M + K_L = 1$. The amplitude of the synthesized virtual voltage vector in the α_1-β_1 subspace is denoted as $|VV_{S1}|$, while the amplitude in the α_5-β_5 subspace is denoted as $|VV_{S5}|$. And to eliminate the harmonic, let the amplitude in the α_5-β_5 subspace be 0, that is

$$|VV_{S5}| = 0 \tag{11}$$

which gives

$$\begin{cases} K_L = 0.578, \ K_M = 0.422 \\ |VV_{S1}| = 0.571U_{\rm dc}. \end{cases} \tag{12}$$

The action time of the long vectors is $0.578T_s$, and the medium vectors is $0.422T_s$. The synthesized virtual vector has an amplitude of $0.571U_{\rm dc}$, which can effectively improve the utilization rate of the bus voltage. Further analysis shows that only by ensuring that the action time of the long vector is 1.3697 times of that of the medium vector, the amplitude of the synthesized voltage vector in the α_5-β_5 subspace becomes 0. Based on the synthesis rules outlined above, the 12 virtual voltage vectors can be synthesized, and the distribution of virtual voltage vectors is shown in Fig. 9(c).

To prevent different effects of a single virtual voltage vector within a sector, the assignment method-I in Fig. 7 is chosen which is indicated by the annotations in Fig. 9(c). Moreover, to reduce the occurrence of harmonics in the current, it is imperative to optimize the pulse sequence of the virtual voltage vector. This optimization ensures that the PWM signal maintains symmetrical around the central axis within a single switching cycle.

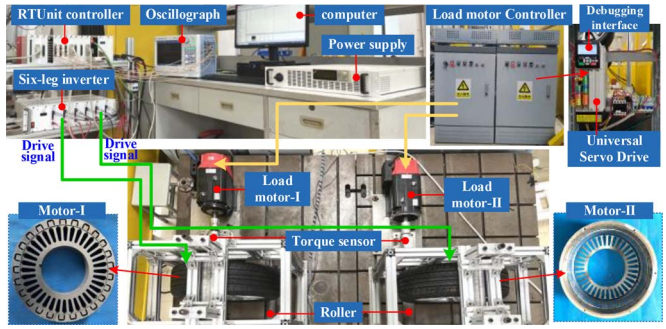

Fig. 10. The photo of experiment platform.

IV. EXPERIMENTAL VERIFICATION

To assess the effectiveness of the integrated direct torque control with MVV modulation, the independent direct torque control (IDTC) [20], [26] is selected as a comparison, and for better implementation of the algorithmic comparison, control variates are realized, where the speed loop parameters are identical, while the prototype of the DIW-PM motors and experimental platform are constructed, as shown in Fig. 10. The experimental setup includes the RTU-204 controller, six-leg inverters and DIW-PM motors experimental platform. It should be noted that the RTU-204 controller core consists of a TMS320F28346 from Texas Instruments Incorporated and four FPGAs from Xilinx Incorporated, and the operating frequency is 5 kHz. And, the load motor-I and load motor-II, powered by the ACS580-C26-17A0-3B universal servo driver, are both induction motors. It is worth noting that the output load torque is transmitted to the in-wheel motor via kinematic equilibrium, facilitated by the

TABLE III
PARAMETERS OF THE EXPERIMENTAL SETUPS

Parameters	Value of Motor-I	Value of Motor-II	Parameters of Load Motor	Value
Flux	0.049 Wb	0.052 Wb	Rated voltage	380 V
L_d	1.253 mH	0.928 mH	Rated power	5.5 kW
L_q	1.642 mH	0.928 mH	Rated torque	35 N·m
Rated speed	900 r/min	900 r/min	Rated speed	1500 r/min
Rated torque	68 N·m	70 N·m	Rated current	13 A
Stator resistance	0.1129 Ω	0.1469 Ω	Maximum speed	8000 r/min
Pole of pairs	25	17	Pole	4
Moment of inertia	1.398 kg·m^2	1 kg·m^2	Rated frequency	51.5 Hz
Proportional	0.5	0.3	Ingress protection	55
Integral	1.5	1.2	/	/

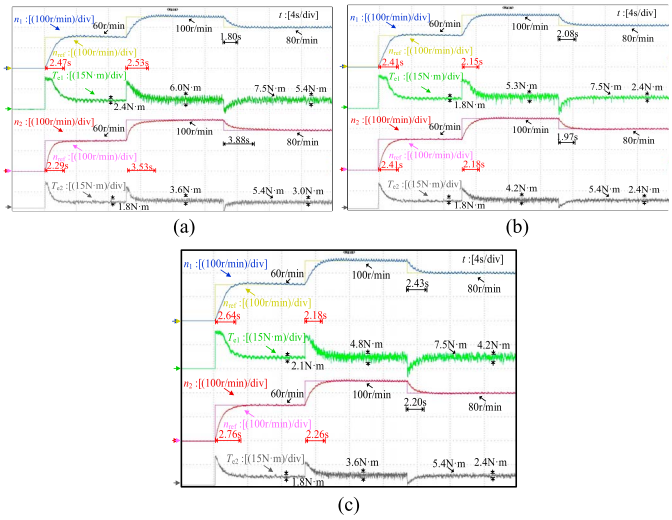

Fig. 11. Waveforms of variable speed experiment. (a) is IDTC, (b) is FR-MVV modulation, (c) is VV-MVV modulation.

frictional torque generated between the roller and the tire as a result of the counter-rotation of both the load motor and the roller. The key parameters of the experimental setups are shown in Table III.

A. Driving Condition Comparison

1) Straight Driving Condition: Figs. 11 and 12 illustrate the experiments conducted on variable speed and variable loads. To replicate actual vehicle driving conditions, the DIW-PM motors are subjected to an initial load, with motor-I and motor-II experiencing loads of 7.5 N·m and 5.4 N·m, respectively. For the convenience of subsequent comparative analysis of the synchronization performance of the proposed algorithm, the absolute value of the setting time difference of the DIW-PM motors during the dynamic process is designated as the indicator for evaluating synchronization performance, defined as the synchronization time difference.

Based on the experiment results in Fig. 11, it is evident that all three algorithms are capable of achieving the desired speed tracking. During the initial phase, IDTC, FR-MVV modulation, and VV-MVV modulation exhibit setting time differences of 0.18 s, 0 s, and 0.12 s, respectively. In comparison to IDTC, the

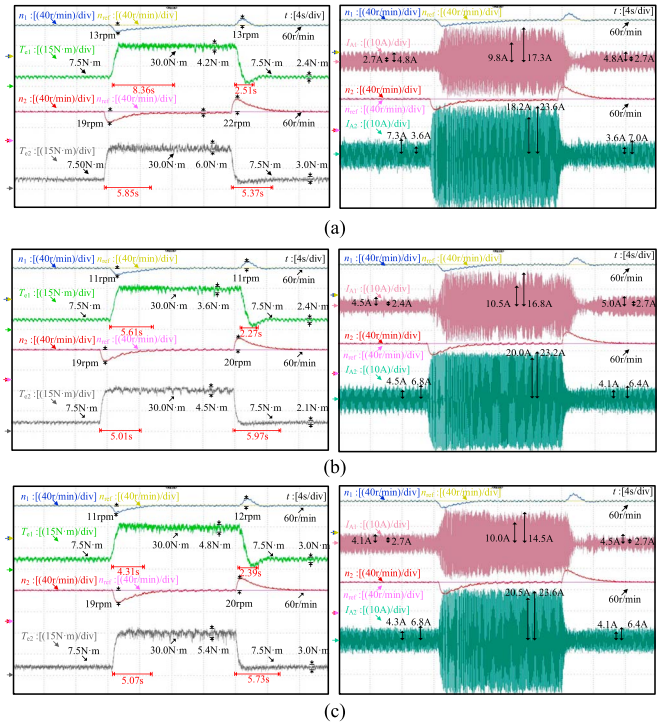

Fig. 12. Waveforms of the torque and current performances. (a) Waveform of IDTC. (b) Waveform of FR-MVV modulation. (c) Waveform of VV-MVV modulation.

dual motor setting time differences of FR-MVV modulation and VV-MVV modulation have reduced by 100.0% and 33.3%, respectively. Furthermore, FR-MVV modulation and VV-MVV modulation have managed to decrease the torque ripple of Motor-I by 25% and 12.5%, while have failed to effectively reduce the torque ripple of motor-II.

During the acceleration condition, the setting time differences of the FR-MVV modulation and VV-MVV modulation method are 0.03 s and 0.08 s, which has a significant reduction of 97% and 92% compared to the IDTC control. In addition, the increased coupling degree of the DIW-PM motors in the FR-MVV modulation method leads to a 16.7% increase in torque ripple for motor-II, compared to the IDTC control. On the other hand, the torque ripple for motor-I in the VV-MVV modulation is measured to be 4.8 N·m, which represents a decrease of 9.4% when compared to the FR-MVV modulation method.

Hence, the experiments have substantiated the effectiveness of the proposed MVV method in achieving accurate speed tracking. Moreover, it has demonstrated that the dynamic synchronization performance of the DIW-PM motors during the variable speed phase is enhanced. The VV-MVV modulation method effectively decreases the torque ripple compared to that of the FR-MVV modulation method, while the synchronization performance is simultaneously improved, which also validates theoretical analysis.

Besides, to evaluate the dynamic responsiveness of the proposed control method including overshoot, setting time, electromagnetic torque ripple, and phase current fluctuations, the comparison experiments of the DIW-PM motors are conducted as shown in Fig. 12.

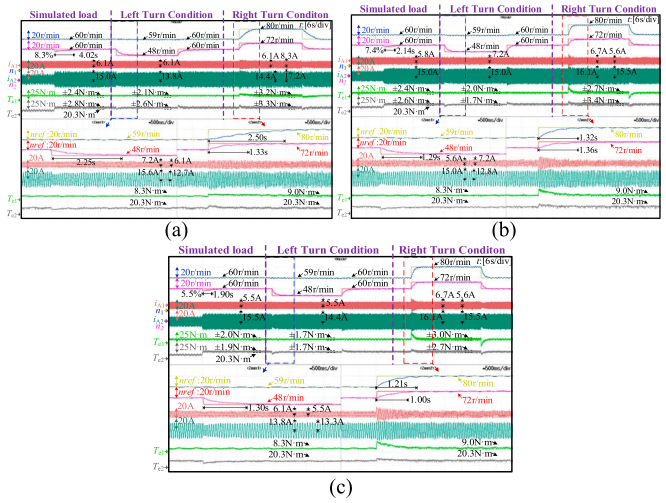

Fig. 13. Waveforms of vehicle steering experiment. (a) IDTC control. (b) FR-MVV modulation. (c) VV-MVV modulation.

The experimental results show that the integrated direct torque control with FR-MVV modulation and VV-MVV modulation significantly reduce time difference when subjected to sudden load increases. Specifically, the synchronization time differences of the FR-MVV modulation and VV-MVV modulation method are 0.6 s and 0.76 s, respectively, which represent a substantial reduction of 76% and 70% compared to the IDTC control. In addition, the phase current ripple of motor-I is reduced by 16% and 40%, and the phase current ripple of motor-II is reduced by 41% and 43%. The results provide evidence for the efficient speed synchronization capabilities of the integrated direct torque control, as well as its effectiveness in resisting interference.

2) Steering Driving Condition: Furthermore, the Ackerman front wheel steering model [27], [28] is adopted to simulated the steering of DDEVs. The actual steering of the vehicle is simulated, with a defined width of 1.9 m and a defined wheelbase of 2.7 m. Assuming that motor-I and motor-II are the left front wheel and left rear wheel, respectively. Therefore, the simulating actual steering driving conditions are conducted as shown in Fig. 13, where the turning angle is set to 30°. And during the left turn phase, the left front wheel speed reduces to 59 r/min and the left rear wheel speed drops to 48 r/min, while the left front wheel speed climbed to 80 r/min and the left rear wheel speed increased to 72 r/min when turning right.

It can be seen that the proposed MVV modulation strategy can significantly reduce setting time and torque ripple under the left turn operating conditions, while the proposed VV-MVV modulation shows better performance, effectively reducing current ripple to 45.4% of motor-I and 82.7% of motor-II. Furthermore, the traditional IDTC algorithm cannot effectively and quickly track commands for the left front wheel under right turn operation conditions, and the vehicle is prone to shaking. However, the proposed MVV modulation strategy effectively responds to instructions of upper layer controller, achieving synchronous speed change of front and rear wheels. MVV modulation and VV-MVV modulation effectively reduce synchronization time difference by 96.5% and 82.1%, respectively.

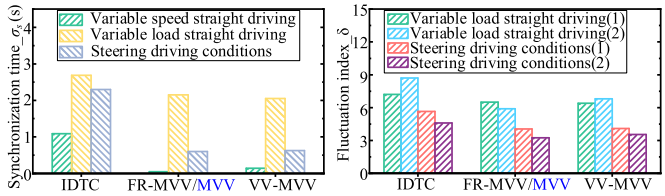

Fig. 14. Comprehensive performance comparison.

TABLE IV
COMPREHENSIVE PERFORMANCE COMPARISON

Items	Controllers		Synchronized Performance	Tracking Performance	Steering Deviation
	UCs	MCs			
[29]	/		/	48.4–62.6%	51.3%
[30]	1	/	/	74%	39.6%
[11]	1	4	/	67.2–84.6%	77%
[31]	1	2	47.6–48.1%	44.3%	/
Proposed	1	2	33–70%	50%	60%

Consequently, the proposed MVV modulation method quickly responds to diverse commands from upper layer controller, while ensuring vehicle stability and improving dynamic performance of motors.

3) Comprehensive Performance Comparison: In conclusion, by integrating Figs. 11–13, a comprehensive performance comparison diagram is shown in Fig. 14. Employing the average synchronization time σ_s and the sum of average torque fluctuation and current fluctuation δ as evaluation principles, and it is important to highlight that (1) corresponds to motor-I, while (2) corresponds to motor-II.

It can be seen from the Fig. 14 that the MVV modulation strategy enhances the cooperative functionality of the DIW-PM motors in diverse complex operational scenarios. Furthermore, it successfully mitigates current and torque ripples in the operation of the front and rear in-wheel motors, thereby enhancing signal transmission stability, ensuring transmission efficiency, and diminishing motor ripple. The robustness of the MVV modulation strategy also effectively shares the computational power of the upper layer controller, improving vehicle handling stability.

Furthermore, compared with other advanced control techniques, the Table IV shows that the method proposed in this article effectively leads to a reduction in the quantity of motor controllers (MCs) under the same number of upper layer controllers (UCs), consequently enhancing the redundancy of the vehicle chassis. The synchronous performance of the multiple in-wheel motors has improved by a range of 33% to 70%. The predetermined trajectory of the vehicle under various operating conditions has also been excellently tracked, and the proposed algorithm, which responds quickly, further demonstrates good performance in real-time implementation.

B. Steady State Performance Comparison

The bus voltage utilization rates of IDTC, FR-MVV modulation, and VV-MVV modulation are displayed in Table V. Particularly, the bus voltage utilization for motor-I of the FR-MVV modulation and VV-MVV modulation methods are improved

TABLE V
COMPREHENSIVE PERFORMANCE COMPARISON

Performance	IDTC	FR-MVV	VV-MVV
Voltage utilization rate of Motor-I	23.35%	28.38%	30.55%
Voltage utilization rate of Motor-II	17.17%	18.52%	25.25%

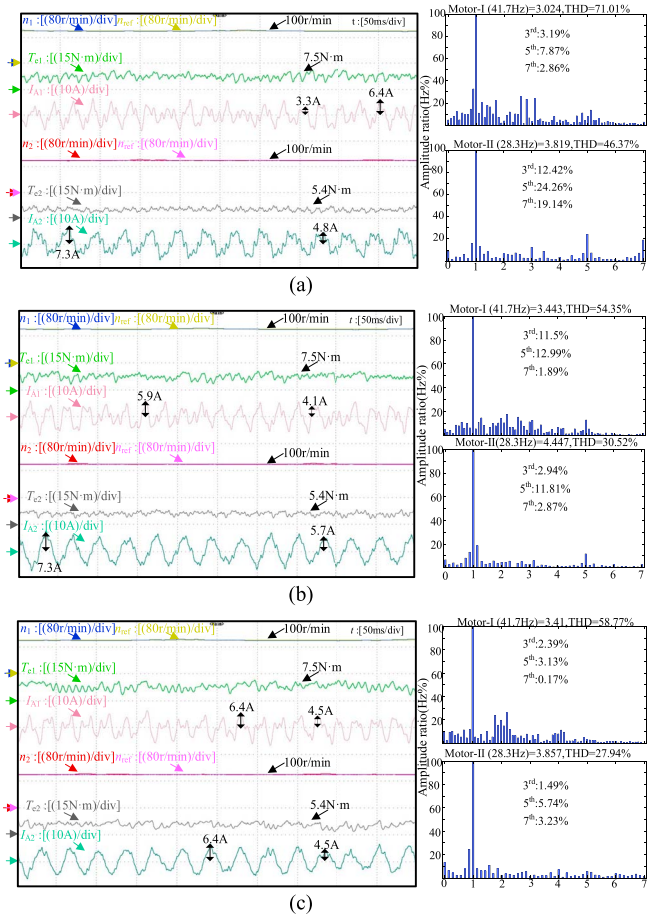

Fig. 15. Experimental waveforms of phase-a current. (a) Current of IDTC control. (b) Current of FR-MVV modulation. (c) Current of VV-MVV modulation.

by 21.5% and 30.8%, respectively, compared to the IDTC. Equally, for motor-II, the bus voltage utilization rates of the FR-MVV modulation and VV-MVV modulation methods have improved by 7.8% and 47.1%, respectively. These findings indicate that the MVV modulation contribute to an improved utilization rate of busbar voltage, although the improvement effect of FR-MVV modulation method is not obvious. Conversely, due to the amplitude of virtual vectors, the VV-MVV modulation method proves to be highly effective in improving bus voltage utilization.

Fig. 15 shows the THD of the phase-a current for different strategies under the condition of the same speed. It can be seen that the proposed algorithms can significantly decrease the phase-a current THD, while VV-MVV modulation method exhibits superior performance in reducing odd harmonic content of current. Specifically, the current THD of FR-MVV modulation and VV-MVV modulation decreased by 16.66% of motor-I and 15.85% of motor-II, 12.24% of motor-I and 18.43% of motor-II, respectively, compared to IDTC. Furthermore, the 3rd, 5th, and 7th harmonic content of the current have been reduced to 1.49%, 5.74%, and 3.23%, respectively, through the application of VV-MVV modulation. Although FR-MVV modulation sacrifices the odd harmonic content of the phase current of front wheel motor to enhance synchronization performance, considering the integrated concept proposed in the manuscript, by summing the odd harmonic content of phase-a current of the front and rear in-wheel motors as an evaluation system, it is evident that both FR-MVV and VV-MVV modulation effectively decrease the total odd phase current harmonic content.

V. CONCLUSION

In this article, a new integrated direct torque control strategy with the multiple voltage vector modulation is proposed for the DD EV system. A 1/2 DD system with DIW-PM motors is selected as the case study to illustrate our proposed design method. The integrated modulation principle is proposed, where the frequency ratio of integrated modulation and virtual vector integrated modulation are designed for the 1/2 DD system. The dual in-wheel PM motor drive system is established and the mathematic model is derived. The integrated direct torque control strategy with MVV modulation is discussed in detail. Compared to the traditional IDTC control, the experimental results show the integrated direct torque control with both the FR-MVV modulation and VV-MVV modulation can effectively enhance the speed synchronization and speed disturbance resistance performance. Additionally, both FR-MVV modulation and VV-MVV modulation are effective in significantly decreasing current THD, while VV-MVV modulation exhibits superior performance in reducing odd harmonic content of current, with the 3rd, 5th, and 7th harmonics reduced to 1.49%, 5.74%, and 3.23%, respectively. Meanwhile, the torque ripple of the VV-MVV modulation is significantly reduced, and the stability of the DD system is improved. The presented study provides a new research path to realize high performance control for the DD systems.

REFERENCES

[1] Y. Hori, "Future vehicle driven by electricity and control-research on four-wheel-motored UOT electric march II," *IEEE Trans. Ind. Electron.*, vol. 51, no. 5, pp. 954–962, Oct. 2004.

[2] L. Xu et al., "Robust Predictive current control of hybrid-excited axial flux-switching PM motor based on multiple-resolution parameter identification," *IEEE Trans. Ind. Electron.*, vol. 71, no. 11, pp. 13708–13719, Nov. 2024.

[3] X. Zhu, Z. Shu, L. Quan, Z. Xiang, and X. Pan, "Design and multi-condition comparison of two outer-rotor flux-switching permanent-magnet motors for in-wheel traction applications," *IEEE Trans. Ind. Electron.*, vol. 64, no. 8, pp. 6137–6148, Aug. 2017.

[4] H. Zhou, F. Jia, H. Jing, Z. Liu, and L. Güvenç, "Coordinated longitudinal and lateral motion control for four wheel independent motor-drive electric vehicle," *IEEE Trans. Veh. Technol.*, vol. 67, no. 5, pp. 3782–3790, May 2018.

[5] S. E. Li, F. Gao, D. Cao, and K. Li, "Multiple-model switching control of vehicle longitudinal dynamics for platoon level automation," *IEEE Trans. Veh. Technol.*, vol. 65, no. 6, pp. 4480–4492, Jun. 2016.
[6] L. Zhai, C. Wang, Y. Hou, and C. Liu, "MPC-Based integrated control of trajectory tracking and handling stability for intelligent driving vehicle driven by four hub motor," *IEEE Trans. Veh. Technol.*, vol. 71, no. 3, pp. 2668–2680, Mar. 2022.
[7] H. Deng, Y. Zhao, A.-T. Nguyen, and C. Huang, "Fault-tolerant predictive control with deep-reinforcement-learning-based torque distribution for four in-wheel motor drive electric vehicles," *IEEE/ASME Trans. Mechatron.*, vol. 28, no. 2, pp. 668–680, Apr. 2023.
[8] W. Cho, J. Choi, C. Kim, S. Choi, and K. Yi, "Unified chassis control for the improvement of agility, maneuverability, and lateral stability," *IEEE Trans. Veh. Technol.*, vol. 61, no. 3, pp. 1008–1020, Mar. 2012.
[9] L. Xu et al., "Multiple-mode current control for a hybrid-excitation axial flux switching permanent magnet motor considering driving cycles," *IEEE Trans. Ind. Electron.*, vol. 71, no. 1, pp. 204–214, Jan. 2024.
[10] Y. Xu, L. Jiang, B. Wei, and L. Qiu, "An optimal torque distribution strategy for four-motorized-wheel electric vehicle considering energy conversation," *IEEE Access*, vol. 8, pp. 135975–135988, 2020.
[11] L. Zhai, T. Sun, and J. Wang, "Electronic stability control based on motor driving and braking torque distribution for a four in-wheel motor drive electric vehicle," *IEEE Trans. Veh. Technol.*, vol. 65, no. 6, pp. 4726–4739, Jun. 2016.
[12] Q. Wang, Y. Zhang, and L. Jin, "Torque coordinated control of four-wheel independent drive electric vehicles in cornering," *Eng. Technol. Ed.*, vol. 37, no. 5, pp. 985–989, 2007.
[13] B. Li et al., "An optimal torque distribution control strategy for four-independent wheel drive electric vehicles," *Vehicle Syst. Dyn.*, vol. 53, no. 8, pp. 1172–1189, 2015.
[14] X. Zhang, D. Göhlich, and J. Li, "Energy-Efficient toque allocation design of traction and regenerative braking for distributed drive electric vehicles," *IEEE Trans. Veh. Technol.*, vol. 67, no. 1, pp. 285–295, Jan. 2018.
[15] C. Liu, H. Liu, L. Han, W. Wang, and C. Guo, "Multi-level coordinated yaw stability control based on sliding mode predictive control for distributed drive electric vehicles under extreme conditions," *IEEE Trans. Veh. Technol.*, vol. 72, no. 1, pp. 280–296, Jan. 2023.
[16] D. Tavernini, M. Metzler, P. Gruber, and A. Sorniotti, "Explicit nonlinear model predictive control for electric vehicle traction control," *IEEE Trans. Control Syst. Technol.*, vol. 27, no. 4, pp. 1438–1451, Jul. 2019.
[17] J. Liang et al., "An energy-oriented torque-vector control framework for distributed drive electric vehicles," *IEEE Trans. Transport. Electrific.*, vol. 9, no. 3, pp. 4014–4031, Sep. 2023.
[18] M. L. De Klerk and A. K. Saha, "A comprehensive review of advanced traction motor control techniques suitable for electric vehicle applications," *IEEE Access*, vol. 9, pp. 125080–125108, 2021.
[19] X. Zhu et al., "Current decoupling model predictive control of a leakage flux controllable PM motor in virtual flux reference frame," *IEEE Trans. Ind. Electron.*, vol. 71, no. 8, pp. 8471–8481, Aug. 2024, doi: 10.1109/TIE.2023.3314862.
[20] F. Niu, B. Wang, A. S. Babel, K. Li, and E. G. Strangas, "Comparative evaluation of direct torque control strategies for permanent magnet synchronous machines," *IEEE Trans. Power Electron.*, vol. 31, no. 2, pp. 1408–1424, Feb. 2016.
[21] D. Lu, J. Zhang, S. Wang, Z. Yuan, and Y. Wu, "Analysis of dynamic and economic performance for electric vehicles with torque coordinated control strategy in CLTC," in *Proc. 26th Int. Conf. Elect. Machines Syst. (ICEMS)*, Zhuhai, China, 2023. pp. 544–549.
[22] Y. Liu et al., "Development of China light-duty vehicle test cycle," *Int. J. Automot. Technol.*, vol. 21, no. 5, pp. 1233–1246, Oct. 2020.
[23] R. Gunabalan, P. Sanjeevikumar, F. Blaabjerg, O. Ojo, and V. Subbiah, "Analysis and implementation of parallel connected two-induction motor single-inverter drive by direct vector control for industrial application," *IEEE Trans. Power Electron.*, vol. 30, no. 12, pp. 6472–6475, Dec. 2015.
[24] Y. Zhao and T. A. Lipo, "Space vector PWM control of dual three-phase induction machine using vector space decomposition," *IEEE Trans. Ind. Appl.*, vol. 31, no. 5, pp. 1100–1109, Sep./Oct. 1995.
[25] G. Grandi, G. Serra, and A. Tani, "Space vector modulation of a six-phase VSI based on three-phase decomposition," in *Proc. Int. Symp. Power Electron. Elect. Drives Automat. Motion*, Ischia, Italy, 2008, pp. 674–679.
[26] Y. Zhang and J. Zhu, "Direct torque control of permanent magnet synchronous motor with reduced torque ripple and commutation frequency," *IEEE Trans. Power Electron.*, vol. 26, no. 1, pp. 235–248, Jan. 2011.
[27] K. Ahiska, M. K. Ozgoren, and M. K. Leblebicioglu, "Energy and time optimal autopilot for electric vehicles performing Ackerman cornering," *IEEE Trans. Intell. Transp. Syst.*, vol. 23, no. 10, pp. 17258–17270, Oct. 2022.
[28] W. Yu, O. Y. Chuy, E. G. Collins, and P. Hollis, "Analysis and experimental verification for dynamic modeling of a skid-steered wheeled vehicle," *IEEE Trans. Robot.*, vol. 26, no. 2, pp. 340–353, Apr. 2010.
[29] Y. Yu, W. Ji, R. Li, A. Lu, and G. Tian, "Vehicle motion control beyond and within the stability limits for 4WD electric vehicles," *IEEE Trans. Intell. Veh.*, vol. 9, no. 1, pp. 2348–2363, Jan. 2024.
[30] S. Liu, L. Zhang, J. Zhang, J. Wang, and C. Ren, "Cooperative control of path tracking and driving stability for intelligent vehicles on potholed road," *IEEE Trans. Intell. Veh.*, vol. 9, no. 1, pp. 2499–2508, Jan. 2024.
[31] S. Zou, W. Zhao, C. Wang, W. Liang, and F. Chen, "Tracking and synchronization control strategy of vehicle dual-motor steer-by-wire system via active disturbance rejection control," *IEEE/ASME Trans. Mechatron.*, vol. 28, no. 1, pp. 92–103, Feb. 2023.

Zhaoheng Wang received the B.Sc. degree in electrical engineering from the School of Electrical Engineering, Southeast University, Nanjing, China, in 2022. He is currently working toward the M.Sc. degree in electrical engineering with Jiangsu University, Zhenjiang, China.

His research interests include control of permanent magnet synchronous motor control and the cooperative control of multiple motors.

Xiaoyong Zhu (Member, IEEE) received the B.Sc. and M.Sc. degrees from Jiangsu University, Zhenjiang, China, in 1997 and 2002, respectively, and the Ph.D. degree in 2008, from the School of Electrical Engineering, Southeast University, Nanjing, China, all in electrical engineering.

His research interests include on the design, analysis and control of the type of hybrid-excited permanent magnet machine.

Since 1999, he has been with Jiangsu University, where he is currently a Professor with the School of Electrical Information Engineering. From 2007 to 2008, he was a Research Assistant with the Department of Electrical and Electronic Engineering, University of Hong Kong, Hong Kong. From 2012 to 2013, he was a Visiting Professor with the Department of Energy-Funded Graduate Automotive Technology Education Center for Electric Drive Transportation, University of Michigan, Dearborn, MI, USA. He has authored or co-authored more than 70 referred technical papers, and holds 12 patents in his research field, which include design and drive control of electric machines with wide-speed range, less rare-earth permanent magnet motor, and multiport permanent magnet motor.

Lei Xu (Member, IEEE) received the B.Sc. degree in electrical engineering and automation from Yancheng Institute of Technology, Yancheng, China, in 2010, the M.Sc. degree from Jiangsu University, Zhenjiang, in 2013, and the Ph.D. degree from the Southeast University, Nanjing, in 2017, both in electrical engineering.

Currently, he is an Associate Professor with the School of Electrical and Information Engineering, Jiangsu University, Zhenjiang, China. His research interests include the high-performance permanent magnet motors, the development of advanced motor control strategies, and their applications in aerospace, automotive engineering, renewable energy generation system, and intelligent manufacturing equipment system.

Wen-Hua Chen (Fellow, IEEE) received the M.Sc. and Ph.D. degrees from the Department of Automatic Control, Northeastern University, Shenyang, China, in 1989 and 1991, respectively.

From 1991 to 1996, he was a Lecturer with the Department of Automatic Control, Nanjing University of Aeronautics and Astronautics, Nanjing, China. From 1997 to 2000, he held a research position and then a lectureship in control engineering with the Centre for Systems and Control, University of Glasgow, Glasgow, U.K. Currently, he is a Professor in autonomous vehicles with the Department of Aeronautical and Automotive Engineering, Loughborough University, Loughborough, U.K. He has authored or co-authored three books and 350 papers in journals and conferences. His research interests include the development of advanced control strategies and their applications in aerospace and automotive engineering, particularly in unmanned electric aircraft and vehicles.

Dr. Chen is a fellow of the Institution of Engineering and Technology and the Institution of Mechanical Engineers. He was the recipient of the EPSRC Established Career Fellowship Award.

Qiyuan Liu received the B.Sc. degree from Shanghai Jiao Tong University, Shanghai, China, in 2022, where he is currently working toward the M.Sc. degree with Jiangsu University, Zhenjiang, China, both in electrical engineering.

His research interests include control of permanent magnet synchronous motor control and the cooperative control of multiple motors.

Li Quan received the B.Sc. degree in electrical engineering from Hefei University of Technology, Hefei, China, in 1985, the M.Sc. degree in motors and electrical specialty from the Southeast University, Nanjing, China, in 1991, and the Ph.D. degree in power electronics and power transmission from Nanjing University of Aeronautics and Astronautics, in 2007.

Since 1998, he has been with Jiangsu University, where he is currently a Professor with the School of Electrical and Information Engineering. He has authored or co-authored more than 100 technical papers, one textbook, and holds three patents in these areas. His teaching and research interests include high performance permanent magnet motor for electric vehicles (EVs), double rotor permanent magnet motor for hybrid electric vehicles (HEVs), and motor drives control.